First-principles study of elastic, electronic, thermodynamic, and thermoelectric transport properties of TaCoSn

Enamul Haque, M. Anwar Hossain[*]

Department of Physics, Mawlana Bhashani Science and Technology University, Santosh, Tangail-1902, Bangladesh

A B S T R A C T

In this paper, we have performed a comprehensive set of first-principles calculations to study elastic, electronic, thermodynamic and thermoelectric properties of TaCoSn using density functional theory (DFT). Half-heusler, TaCoSn has been found to be elastically and thermodynamically stable, ductile and hard material. The Debye temperature of TaCoSn has been found to be 375.39 K. The calculated energy bands indicate that TaCoSn is an indirect band gap semiconductor and the value of gap is 1.107 eV using PBE functional and it is 1.153 eV by TB-mBJ potentials. Such small increase of band gap by TB-mBJ potential has no significant effect on the transport properties of TaCoSn. In TaCoSn, no significant spin-orbit interaction is found. The density of states at the Fermi energy is dominated by Ta-5d and Co-3d orbitals due to strong hybridization between them. We also calculate the relaxation time and lattice thermal conductivity. The lattice thermal conductivity of TaCoSn (4.95 W/mK at 300 K) is relatively small than that of other half-heusler compounds. The maximum Seebeck coefficient at 500 K is 249.41 μV/K. The obtained power factor ($S^2\sigma/\tau$) at 600 K is $\sim 12.5 \times 10^{11}$ W/msK^2. The calculated maximum figure of merit (ZT) is 0.73 at 600 K indicates that TaCoSn is a promising material for thermoelectric device applications.

Introduction

Thermoelectric energy generation (TEG) might be the alternative way to solve the 21st century energy crises as this method does not require fossil-fuels and is thus environment friendly. TEG is an encouraging and effective technology for power generation and cooling. Thermoelectric materials are used to convert heat to electricity and vice-versa. The coefficient of performance of a potential thermoelectric material is determined by the dimensionless figure of merit, $ZT = \frac{S^2\sigma T}{k}$, where S, σ, $k = k_e + k_l$ and T are the Seebeck coefficient, electrical conductivity, thermal conductivity (consisting of electronic and lattice thermal conductivity) and absolute temperature, respectively. The half-heusler 18-electron ABX compounds have attracted much attention due to their semiconducting behavior [1] and high thermoelectric performance [2–5]. Recently, researchers reported some previously unknown Half-Heusler compounds, such as ScPtBi, TiPdSn, ZrNbPb, etc. [6–9] and it is found that ZrNiPb based half-heusler materials can exhibit high thermoelectric performance (ZT ~ 0.8 at 800 K) [4]. Although the pure ZrNiPb has low thermoelectric performance, the doping of suitable element (Sn, Bi) significantly increases the ZT of ZrNiPb [4]. Recently, Zakutayev et al. reported the experimental synthesis of TaCoSn, an 18-electron ABX half-heusler compound [10]. This material was reported

to be semiconductor and possibility of high thermoelectric performance [11]. Bhattacharya et al. calculated the optimal zT_0 (not usual ZT) of TaCoSn by assuming the lattice part of thermal conductivity $\kappa_{ph}/\tau \sim 10^{14}$ W/mKs and found to be 1.73 [11]. This indicates the possibility of high thermoelectric performance. Therefore, it is reasonable to study the lattice thermal conductivity and details of transport properties along with the electronic nature of TaCoSn.

In this paper, we have presented first-principles study of elastic, electronic, thermodynamic and thermoelectric transport properties of TaCoSn by using density functional theory (DFT) [12] and semi-classical Boltzmann transport theory. We have calculated elastic constants and moduli of elasticity, anisotropy, Vickers hardness. We also calculate the Debye temperature of TaCoSn which found to be 375.39 K. The calculated band structure of TaCoSn confirms the semiconducting nature and the possibility of high thermoelectric performance. The relaxation time and lattice thermal conductivity have been calculated for TaCoSn. The maximum Seebeck coefficient is obtained at 500 K, 249.41 μV/K and power factor ($S^2\sigma$) of TaCoSn is 2.22×10^{12} W/msK^2 at 1000 K. The calculated maximum thermoelectric figure of merit (ZT) is found to be 0.731 at 600 K indicating that TaCoSn is a high performance thermoelectric material.

---

[*] Corresponding author.
E-mail address: anwar647@mbstu.ac.bd (M.A. Hossain).

Computational methods

The elastic properties of TaCoSn were calculated by using IRelast method [13] as interfaced with the full potential linearized augmented plane wave (LAPW) method as implemented in WIEN2k [14]. The electronic properties, such as density of states (DOS), band-structure, were calculated in WIEN2k. To obtain a good convergence basis set, a plane wave cut off of kinetic energy $RK_{max} = 7.0$ was selected by convergence test. A mesh of dense ($21 \times 21 \times 21$) k-points was used in the elastic and electronic properties calculations for BZ integrations. The generalized gradient approximation (GGA) within the Perdew-Burke-Ernzerhof (PBE) [15,16] scheme was utilized for elastic properties calculation. The PBE-GGA and Tran-Blaha modified Becke-Johnson potentials (TB-mBJ) [17] were used for electronic and transport calculations. We also performed electronic and transport properties including spin-orbit interactions (SOC) among all atoms. The transport properties were explored by solving Boltzmann semi-classical transport equations as implemented in BoltzTraP [18]. A denser mesh ($43 \times 43 \times 43$) of k-points was used for thermoelectric transport properties calculations. The transport parameters were calculated at the chemical potential, which is equal to the zero temperature Fermi energy. The lattice thermal conductivity and relaxation time were calculated by using the finite displacement approach [19,20] as implemented in Phono3py [21]. The $2 \times 2 \times 2$ supercell was created and a mesh of $4 \times 4 \times 4$ cubic shifted k-points were used for harmonic and anharmonic forces calculation. The force calculation was performed in Quantum espresso package [22] by using the same PBE functional, 35 Ry cutoff energy for wave functions, and ultrasoft pseudopotentials. Then, the lattice thermal conductivity was calculated by performing BZ integration in the q-space with $21 \times 21 \times 21$ mesh and the equation $\kappa = \frac{1}{NV} \sum_\lambda C_\lambda \boldsymbol{v}_\lambda \otimes \boldsymbol{v}_\lambda \tau$, where V is the volume of the unit cell, $\boldsymbol{v}$ is the group velocity, τ is the SMRT for the phonon mode λ, and C_λ is mode dependent phonon heat capacity. The relaxation time (τ) was calculated from the self-energy ($\Gamma(\omega)$) as found in the above calculation by using $\tau = \frac{1}{2\Gamma(\omega)}$. The Phono3py program has successfully predicted the lattice thermal conductivity of many materials [23–27].

Result and discussions

The equilibrium crystal structure of TaCoSn is shown in Fig. 1. The TaCoSn is a face-centered cubic crystal with space group $F\bar{4}3m$ (#216). The occupied Wyckoff positions for Ta, Co and Sn atoms are 4a (0, 0, 0),
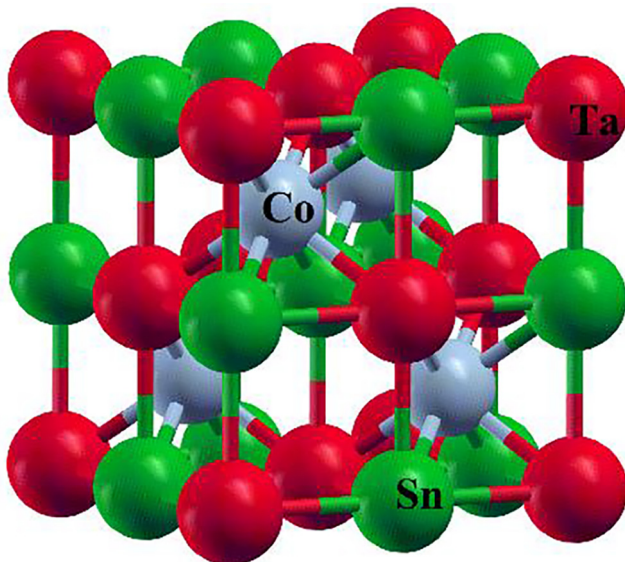

Fig. 1. The crystal structure of TaCoSn.

4b (0.25, 0.25, 0.25) and 4c (0.5, 0.5, 0.5), respectively [10]. The optimized lattice parameter is 5.95 Å which is very close to the experimental (5.94 Å) [10] and the theoretically predicted [6] value (5.97 Å).

Elastic properties

The elastic properties are related to the mechanical stability of a material and hence are important for different practical applications. The anisotropy, hardness, ductility, etc. of a material can be calculated from elastic constants. The strength of a material is measured by the bulk modulus, shear modulus, Young's modulus, and Poisson's ratio. The Reuss [28], shear (G_R), and Voigt [29] shear modulus (G_V) of a cubic crystal are given by: $G_R = \frac{5(c_{11}-c_{12})c_{44}}{4c_{44}+3(c_{11}-c_{12})}$ and $G_V = \frac{c_{11}-c_{12}+3c_{44}}{5}$. The bulk modulus for a cubic crystal can be calculated by the relation $B = \frac{c_{11}+2c_{12}}{3}$. Then, we use the Hill average scheme to find the shear modulus (G) [30]. The Young's modulus (E) and Poisson's ratio (ν) are given by: $E = \frac{9BG_X}{3B+G_X}$ and $\nu = \frac{3B-E}{6B}$. Here, X stands for Reuss (R), Voigt (V) and Hill (H) scheme. The melting temperature is an important parameter for a crystal to use in heating systems. It can be predicted by the following expression [31] $T_m = [553\ K + (5.91\ K/GPa)c_{11}] \pm 300\ K$.

The calculated elastic constants, moduli of elasticity, Poisson's ratio, and melting temperature of TaCoSn are listed in Table 1. The necessary and sufficient conditions of stability for a cubic crystal system are given as:

$$C_{11}-C_{12} > 0; \quad C_{11}+2C_{12} > 0; \quad C_{44} > 0$$

Our calculated elastic constants indicate that TaCoSn crystal is elastically stable. The calculated melting temperature of TaCoSn is high (Table 1). Thus, this material is suitable for high temperature applications. The ductile (or brittle) nature of a material can be found by calculating the Pugh ratio [32]. A material is ductile if the Pugh ratio (B/G) > 1.75, otherwise it is brittle. The calculated value of Pugh ratio is greater than 1.75, hence TaCoSn is a ductile material. A ductile material has a wide range of applications in the parts of machine undergoing rapid acceleration. The calculated Poisson's ratio of TaCoSn (0.3) is in the range of values for metals. The percentage anisotropy that measures the elastic anisotropy and can be calculated by using the expression [33], $A_G = \frac{G_V - G_R}{G_V + G_R}$. The shear elastic anisotropy can be calculated by the following equation [34], $A = \frac{2c_{44}}{c_{11}-c_{12}}$. The value of A_G and A is 0.9% and 0.76, respectively, indicating the material is anisotropic. The Vickers hardness can be calculated by using the following empirical formula [35], $H_V = 2\left(\left(\frac{G}{B}\right)^2 G\right)^{0.585} - 3$. The calculated value of H_V (8.22 GPa) indicates the material to be hard.

Thermodynamic properties

Phonons are the normal mode of quantum vibrations and determine the crystal structure stability. For a stable crystal structure, no imaginary frequency exist for any phonon, the frequency must be real quantity [36,37]. From Fig. 2(a), it is clear that no imaginary frequency exists for TaCoSn throughout the considered BZ. Therefore, TaCoSn is thermodynamically stable. The total phonon density of states is illustrated in Fig. 2(b). The phonon DOS is consistent with the phonon dispersions relations. The Debye temperature of a material is connected to thermal stability and lattice thermal conductivity. The Debye temperature is given by [38]

$$\theta_D = \frac{h}{k_B}\left(\frac{3N}{4\pi V}\right)^{1/3}\left[\frac{1}{3}\left(\frac{2}{v_t^3} + \frac{1}{v_l^3}\right)\right]^{-\frac{1}{3}}$$

where v_l and v_t are (longitudinal and transverse wave velocity, respectively) given by $v_l = \left(\frac{3B+4G}{3\rho}\right)^{1/2}$, $v_t = \left(\frac{G}{\rho}\right)^{1/2}$. The calculated Debye temperature is 375.39 K. The variations of thermodynamic parameters such as bulk modulus (B), heat capacity (C_V), entropy (S), Debye temperature (Θ_D), and Grüneisen parameter (γ) with pressure are shown in

Table 1
The evaluated elastic constants and moduli of elasticity in GPa, Poisson's ratio and melting temperature in K.

c_{11}	c_{12}	c_{44}	B	G_R	G_V	G_H	E_R	E_V	E_H	v	B/G_H	$T_M \pm 300$
382.2	148	88.8	226.2	98.3	100.1	99.2	257.6	261.7	259.6	0.3	2.2	2832

Fig. 3. The bulk modulus sharply increases with increasing pressure but slowly decreases with temperature. The pressure compacts the structure and increases its resistance to external effect, thus, bulk modulus increases with pressure. However, temperature creates vibrations within the crystal and thus, the bulk modulus slowly decreases with increasing temperature. The heat capacity decreases with both temperature and pressure as shown in Fig. 3(b). The entropy measures the degree of disorderness in the crystal structure. The pressure reduces the disorderness in the structure while temperature increases it. Thus, the entropy of TaCoSn increases with temperature but decreases with pressure (See Fig. 3(c)). The Debye temperature is inversely related to the vibrational frequency and thus increases with pressure. However, it slowly decreases with temperature as expected. Note that the Debye temperature calculated by using quasi-harmonic Debye model (385.15 K) is reasonably close to the value calculated from elastic properties within standard Debye model. The Grüneisen parameter determines the anharmonicity and hence phonon scattering. The Small Grüneisen parameter indicates the small phonon scattering which may lead to large contributions to the lattice thermal conductivity. The Grüneisen parameter decreases with pressure but increases with temperature as expected.

Electronic properties

The energy bands of TaCoSn is shown in Fig. 4. The bands are non-dispersive and no overlapping between the valence band and conduction band occurs at the Fermi level. Thus, this indicates semiconducting behavior of TaCoSn. Note that the band gap obtained using PBE-GGA potential is slightly smaller than that obtained by PBE + mBJ potential. Our calculated band structure of TaCoSn using PBE-GGA potential is consistent with others previous result [11]. The value of bandgap is 1.107 eV by using PBE-GGA and 1.153 eV by PBE + mBJ. This band gap is much larger than that of TiPdSn (0.48 eV) obtained using pseudo-potential method [39]. The energy bands indicate that TaCoSn is an indirect band gap. The energy bands of TaCoSn are mainly d-like character, although Sn-p orbitals have large contributions as indicated in Fig. 5(b). The band gap mainly arises from the Ta-5d orbitals. The energy bands of TaCoSn are flat. The flat energy bands are suitable to exhibit high performance thermoelectric properties. It is interesting to note that spin-orbit interactions have no significant effect on the electronic properties of TaCoSn as shown in Fig. 4(c), although significant effects have been found for some other half-Heusler compounds [40]. The band structure remains same as obtained by PBE-mBJ potential. The total, atomic, and projected density of states are shown in Fig. 5. The upper peak in the density of states, from −2 to −1 eV, comes from the strong hybridization between Ta-5d and Co-3d orbitals. This can be well explained by sigma bonding combinations of Ta-5d and Co-3d orbitals. The lower peak, from 1 to 3 eV, arises from the corresponding anti-bonding combinations. The bonds of TaCoSn are covalent due to strong hybridization between Ta-5d and Co-3d orbitals and ionic character due to the relative quantities of DOS of two states. The Ta-5d and Co-3d orbitals have dominant contributions to the density of states at the Fermi level. However, Sn-5p orbitals also have significant contributions to the density of states. The total density of states at the
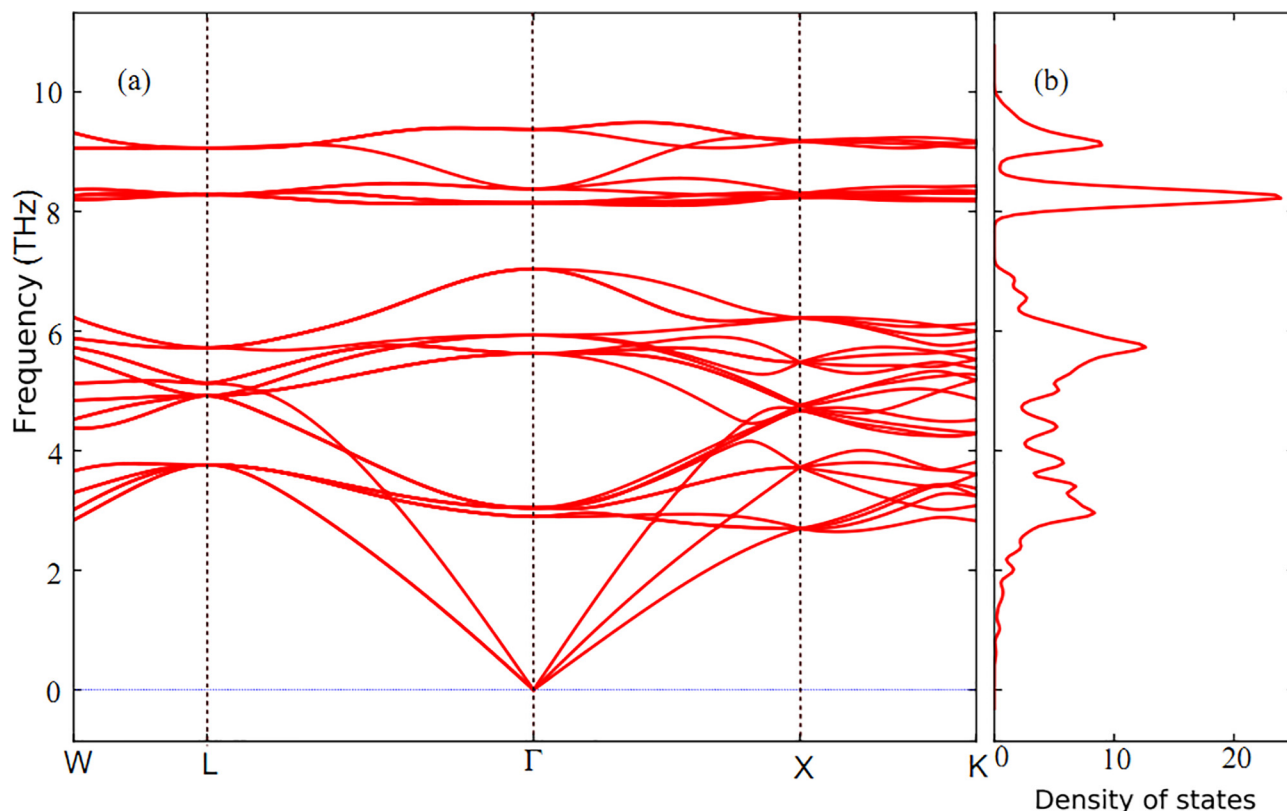
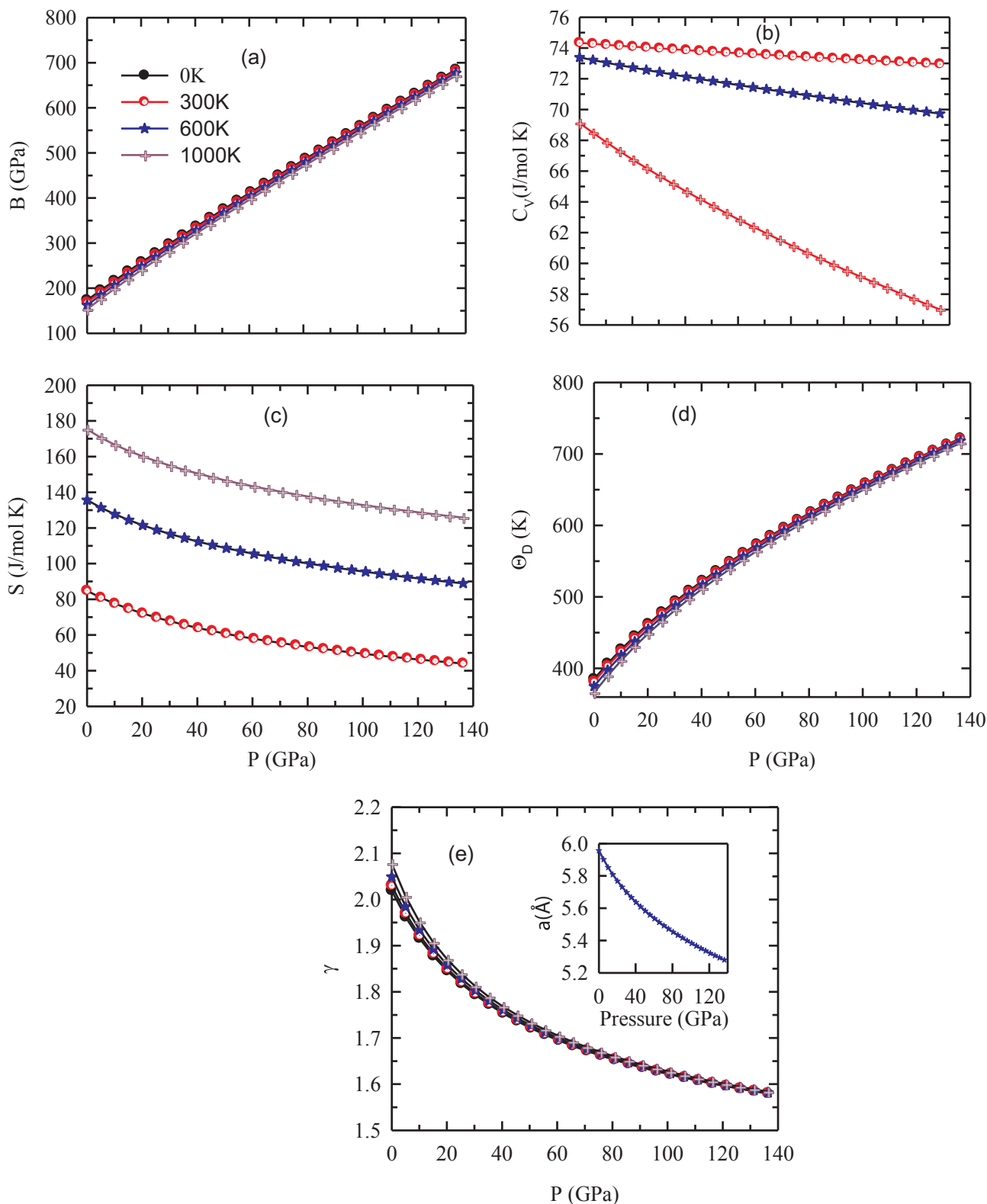**Fig. 2.** Phonon dispersions and total phonon density of states (in arbitrary unit).

Fig. 3. Variations of different thermodynamic quantities with pressure at different temperature: (a) bulk modulus (B), (b) heat capacity (C_V), (c) entropy (S), (d) Debye temperature (Θ_D), and (e) Grüneisen parameter (γ); inset figure shows pressure dependent lattice parameter. We see that Grüneisen parameter decreases with the increase of pressure as lattice parameters decrease.

Fermi level is small and the value is 2.32 states/eV.f.u. The Sommerfeld coefficient is 0.42 mJ/mol.K^2 which is also very small. The density of states gives further confirmation that TaCoSn is a bulk gap semi-conductor.

Thermoelectric properties

The semiconductors with flat valence band and conduction band are expected for good thermoelectric materials. Our calculated band
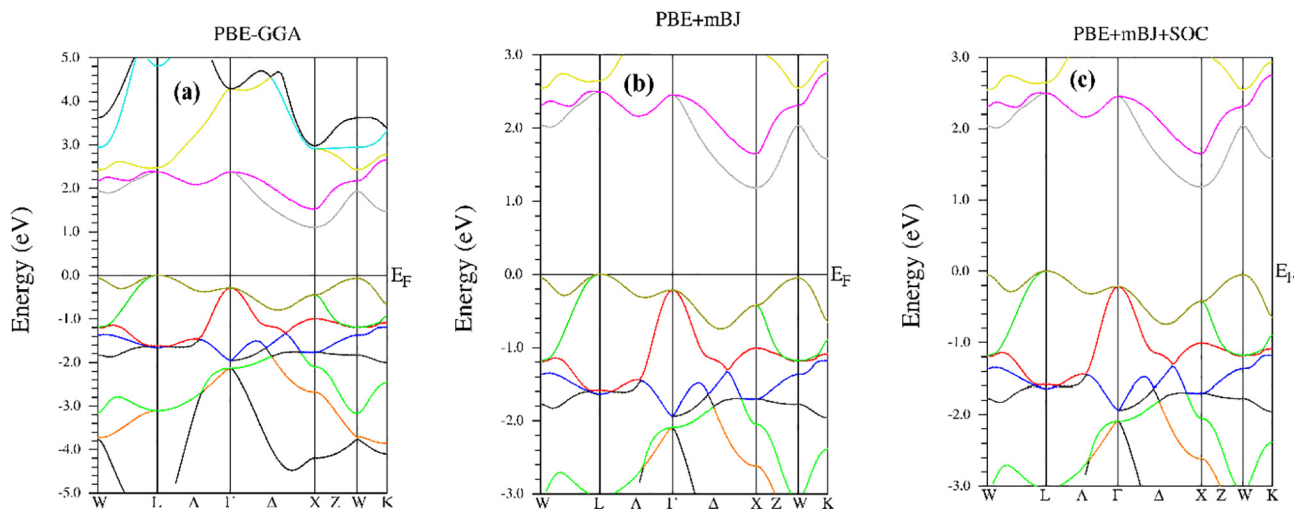
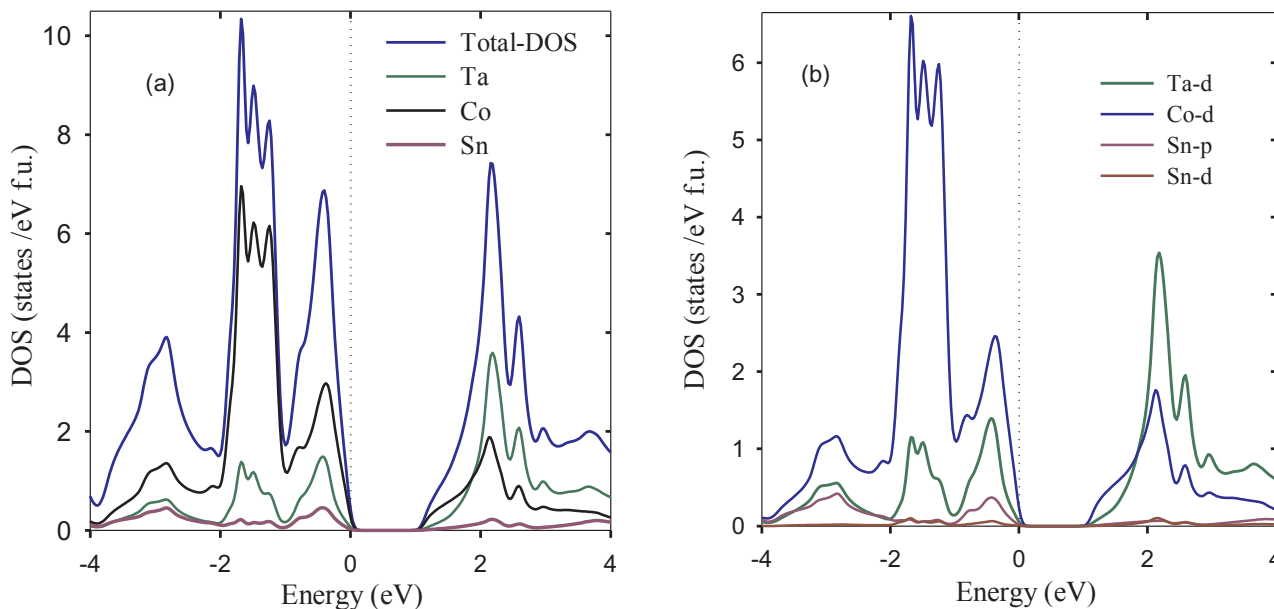**Fig. 4.** Band structure of TaCoSn: (a) PBE + GGA, (b) PBE + mBJ, and (c) PBE + mBJ + SOC.

Fig. 5. Density of states (DOS) of TaCoSn: (a) total and atomic DOS and (b) projected DOS (PDOS).
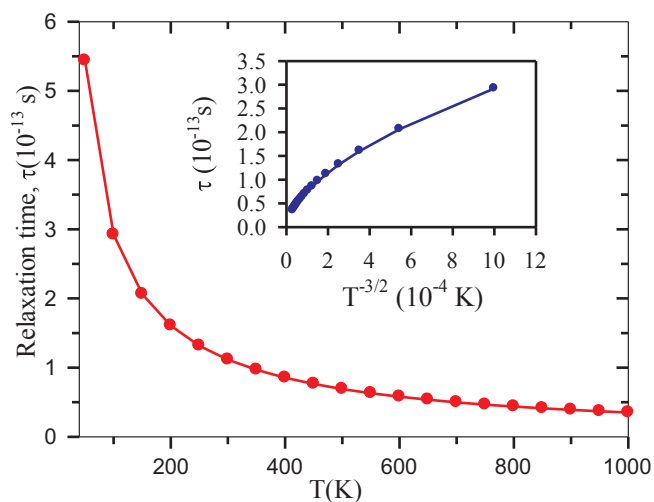

Fig. 6. Phonon Relaxation time with temperature.

structure confirms that TaCoSn is an indirect band gap semiconductor with flat valence and conduction band. Furthermore, the density of states confirms the bulk gap between valence and conduction band. Recently, Zeeshan et al. predicted good thermoelectric performance in TaCoSn without considering lattice thermal conductivity [41]. Therefore, it is reasonable to study the thermoelectric transport properties considering lattice part of the thermal conductivity. Fig. 6 shows the variation relaxation time of TaCoSn with temperature. The calculated relaxation time (by using the linewidths of phonons self-energy [42]) is slightly larger than that obtained for TiPdSn (by Bardeen and Shockley formula [43]) [39]. The relaxation time decreases with increasing temperature due to the increase of phonon scattering. Above Debye temperature, the relaxation time shows $T^{-3/2}$ dependence [44] as illustrated in inset figure of (a). Such linear dependence (inset figure) implies that the acoustic phonon scattering is predominant process in TaCoSn. Gonzalez Romero et al. suggested that $T^{-3/2}$ dependence may be used to find the relaxation time at different temperature [45]. The relaxation time at 300 K is 0.112×10^{-14} s. The Seebeck coefficient (S) of TaCoSn within the temperature range from 50 to 1000 K is shown in Fig. 7(a). The Seebeck coefficient increases sharply up to 500 K and
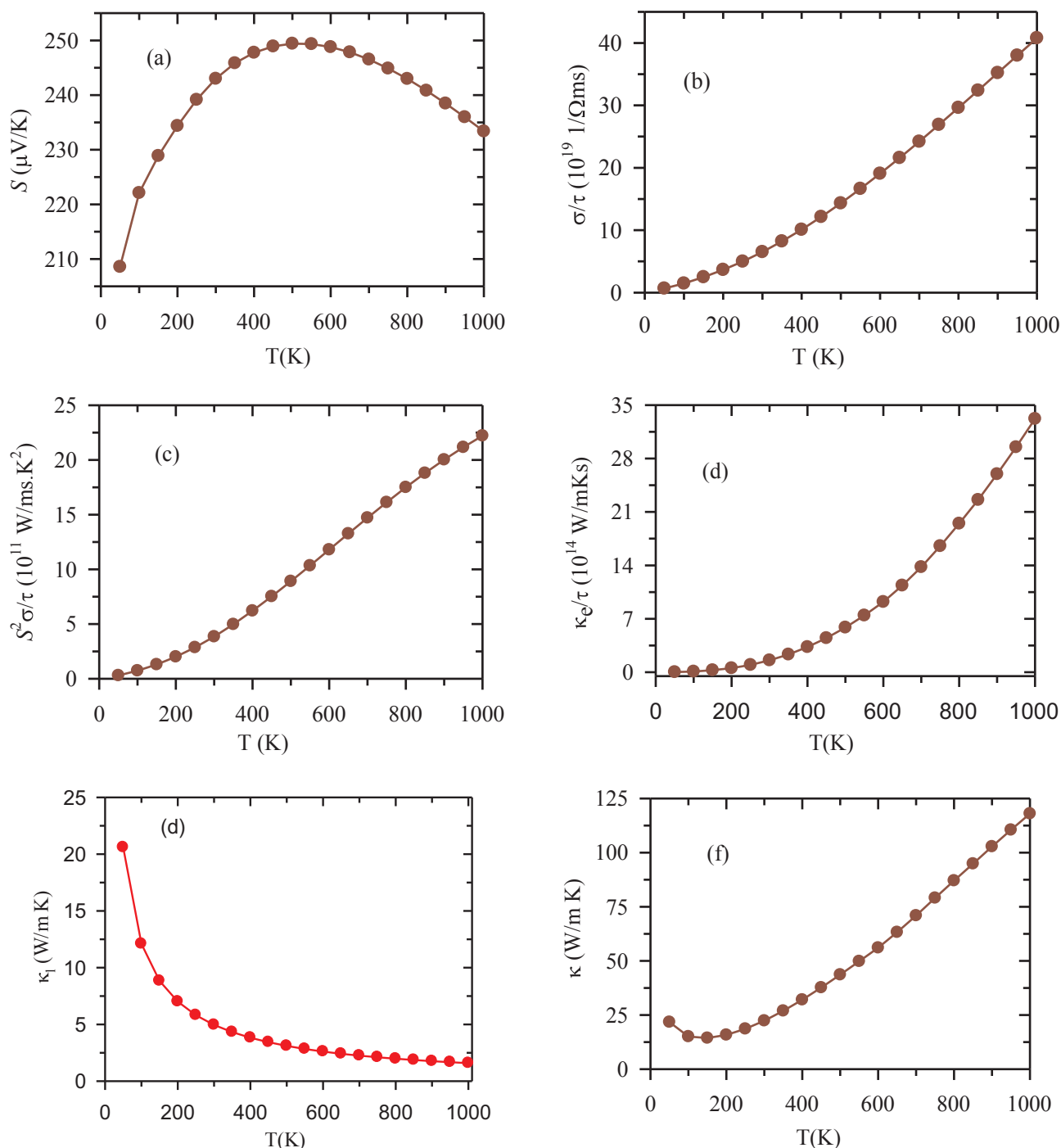
Fig. 7. Temperature dependence of different thermoelectric parameters: (a) Seebeck coefficient (*S*), (b) electrical conductivity (σ/τ), (c) power factor ($S^2\sigma/\tau$), (d) electronic thermal conductivity (κ_e/τ), (e) lattice thermal conductivity (κ_l) and (f) total thermal conductivity.

then decrease gradually. The positive Seebeck coefficient indicates that TaCoSn is p-type material. The maximum Seebeck coefficient obtained at 500 K is 249.41 µ V/K which is much smaller than that of TiPdSn [39]. The variation of electrical conductivity with temperature is shown in the Fig. 5(b). The electrical conductivity (σ/τ) increase slowly up to 600 K and then after it increases sharply. This behavior indicates the semiconducting nature of TaCoSn. The calculated electrical conductivity of TaCoSn at 300 K is $7.28 \times 10^5\, 1/\Omega\mathrm{m}$ which is reasonably close to the value of TiPdSn ($5.13 \times 10^5\, 1/\Omega\mathrm{m}$) [39] but much higher than that of ZrRhBi ($8.74 \times 10^4\, 1/\Omega\mathrm{m}$) [5]. The calculated maximum power factor ($S^2\sigma/\tau$) of TaCoSn at 1000 K is $2.22 \times 10^{12}\, \mathrm{W/msK^2}$ which is higher than that of TiPdSn ($1.488 \times 10^{12}\, \mathrm{W/msK^2}$).

The electronic part of thermal conductivity (κ_e/τ) at a different temperature is illustrated in Fig. 7(d). The electronic thermal conductivity also increases with the temperature slowly up to 650 K and then after increases very fast. The calculated electronic thermal conductivity at 300 K is 17.41 W/mK which is reasonably close to that of TiPdSn (20 W/mK) [39] although, at a higher temperature, the difference is large. The lattice thermal conductivity of TaCoSn is shown in Fig. 5(e). The lattice thermal conductivity decreases sharply with temperature up to 150 K due to the abrupt increase of large phonon vibrations and then decreases slowly. The calculated lattice thermal conductivity of TaCoSn at 300 K is 4.95 W/mK, which is reasonably close to the value obtained for TiPdSn is presented in Table 2. The

Table 2
The thermoelectric properties of TaCoSn at 300 K.

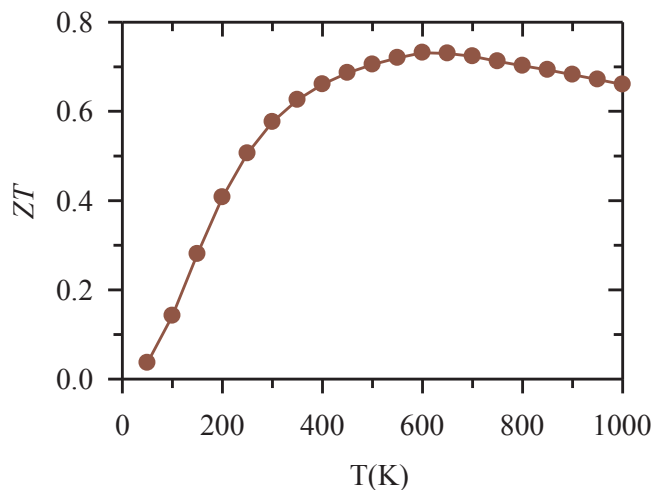|	S (μV/K)	σ (1/Ωm)	$S^2\sigma/\tau$ (W/mK²s)	κ_e (W/mK)	κ_l (W/mK)
TaCoSn	243	7.28×10^5	3.85×10^{11}	17.41	4.95
TiPdSn [31]	≈317	≈5.49×10^5	–	20.01	5.47

Fig. 8. Thermoelectric figure of merit of TaCoSn.

temperature dependence of total thermal conductivity is presented in Fig. 7(f). The thermal conductivity increases with the increase in temperature.

The dimensionless figure of merit of TaCoSn has been calculated by plugging the desired quantities in $ZT = \frac{S^2(\sigma/\tau)}{(k_e/\tau)+k_l}T$, is depicted in Fig. 8. Note that the electrical conductivity and electronic thermal conductivity have been calculated by multiplying the relaxation time of the corresponding temperature $(((\sigma/\tau) \times \tau)$ and $((k_e/\tau) \times \tau))$. We see that ZT increase with increasing temperature up to 600 K and after then it decreases slowly. The calculated maximum ZT value at 600 K is 0.73 which is very close to that for TiPdSn [39], indicates that TaCoSn could be a high performance thermoelectric material. We are conscious of the recent works on this compound, such as transport [41] and defect calculations [11], applications of TaCoSn and its alloy in thermoelectric generator [46]. They used completely different approach and different purpose of the work than from this work. Note that we also calculate the thermoelectric properties using PBE + mBJ and PBE + mBJ + SOC potentials but are not presented here since no significant changes were found in these calculations.

Conclusions

In summary, we have performed first principles calculations to study elastic, electronic, thermodynamic, and thermoelectric properties of TaCoSn, a high performance thermoelectric material, using density functional theory (DFT), and semi-classical Boltzmann transport theory for transport properties. The TaCoSn half-heusler has been found to be elastically stable, ductile in nature. The calculated Vickers hardness indicates that TaCoSn is relatively hard material. The Debye temperature of TaCoSn has been found to be 375.39 K. The calculated energy bands indicate that TaCoSn is an indirect band gap semiconductor and the value of gap is 1.107 eV using PBE and 1.153 PBE + mBJ potentials, with no significant effect of spin-orbit interactions. Such small increase of band gap due to TB-mBJ potential calculation has no significant effect on transport properties. Thus, no significant spin-orbit interaction is present in TaCoSn. The Ta-5d and Co-3d orbitals have dominant contributions to the density of states due to strong hybridization

between them. We also calculate the relaxation time and lattice thermal conductivity using the finite displacement approach. The lattice thermal conductivity of TaCoSn (4.95 W/m K at 300 K) is relatively smaller than that of other half-heusler compounds. The maximum Seebeck coefficient at 500 K is 249.41 μ V/K and power factor ($S^2\sigma$) of TaCoSn is 2.22×10^{12} W/msK² at 1000 K. The calculated maximum merit of figure (ZT) is 0.731 at 600 K. Therefore, TaCoSn is a potential candidate for thermoelectric device applications.

References

[1] Jung D, Koo H-J, Whangbo M-H. Study of the 18-electron band gap and ferromagnetism in semi-Heusler compounds by non-spin-polarized electronic band structure calculations. J Mol Struct Theochem 2000;527:113–9.
[2] Guo S-D. Thermoelectric properties of half-Heusler ZrNiPb by using first principles calculations. RSC Adv 2016;6:47953–8.
[3] Wang G, Wang D. Electronic structure and thermoelectric properties of Pb-based half-Heusler compounds: ABPb (A= Hf, Zr; B= Ni, Pd). J Alloy Compd 2016;682:375–80.
[4] Mao J, Zhou J, Zhu H, Liu Z, Zhang H, He R, et al. Thermoelectric Properties of n-type ZrNiPb-Based Half-Heuslers. Chem Mater 2017;29:867–72.
[5] Kangsabanik J, Alam A. others, Bismuth based half-Heusler alloys with giant thermoelectric figures of merit. J Mater Chem A 2017;5:6131–9.
[6] Gautier R, Zhang X, Hu L, Yu L, Lin Y, Sunde TOL, et al. Prediction and accelerated laboratory discovery of previously unknown 18-electron ABX compounds. Nat Chem 2015;7:308–16.
[7] Abid OM, Menouer S, Yakoubi A, Khachai H, Bin Omran S, Murtaza G, et al. Structural, electronic, elastic, thermoelectric and thermodynamic properties of the NbMSb half heusler (M= Fe, Ru, Os) compounds with first principle calculations. Superlattices Microstruct 2016;93:171–85.
[8] Bencherif K, Yakoubi A, Della N, Abid OM, Khachai H, Ahmed R, et al. First principles investigation of the elastic, optoelectronic and thermal properties of XRuSb: (X= V, Nb, Ta) semi-heusler compounds using the mBJ exchange potential. J Electron Mater 2016;45:3479–90.
[9] Ahmad M, Murtaza G, Khenata R, Bin Omran S, Bouhemadou A, et al. Structural, elastic, electronic, magnetic and optical properties of RbSrX (C, SI, Ge) half-Heusler compounds. J Magn Magn Mater 2015;377:204–10.
[10] Zakutayev A, Zhang X, Nagaraja A, Yu L, Lany S, Mason TO, et al. Theoretical prediction and experimental realization of new stable inorganic materials using the inverse design approach. J Am Chem Soc 2013;135:10048–54.
[11] Bhattacharya S, Madsen GKH. A novel p-type half-Heusler from high-throughput transport and defect calculations. J Mater Chem C 2016;4:11261–8.
[12] Hohenberg P, Kohn W. Inhomogeneous electron gas. Phys Rev 1964;136:B864.
[13] Jamal M. IRelast and 2DR-optimize packages are provided by M. Jamal as part of the commercial code WIEN2K 2014.
[14] Blaha P, Schwarz K, Madsen GKH., Kvasnicka D, Luitz J. wien2k, An Augment. Pl. Wave+ Local Orbitals Progr. Calc. Cryst. Prop. (2001).
[15] Perdew JP, Burke K, Ernzerhof M. Generalized gradient approximation made simple. Phys Rev Lett 1996;77:3865.
[16] Perdew JP, Ruzsinszky A, Csonka GI, Vydrov OA, Scuseria GE, Constantin LA, et al. Restoring the density-gradient expansion for exchange in solids and surfaces. Phys Rev Lett 2008;100:136406.
[17] Tran F, Blaha P. Accurate band gaps of semiconductors and insulators with a semilocal exchange-correlation potential. Phys Rev Lett 2009;102:226401.
[18] Madsen GKH, Singh DJ. BoltzTraP. A code for calculating band-structure dependent quantities. Comput Phys Commun 2006;175:67–71.
[19] Esfarjani K, Stokes HT. Method to extract anharmonic force constants from first principles calculations. Phys Rev B 2008;77:144112.
[20] Parlinski K, Li ZQ, Kawazoe Y. First-principles determination of the soft mode in cubic ZrO2. Phys Rev Lett 1997;78:4063.
[21] Togo A, Chaput L, Tanaka I. Distributions of phonon lifetimes in Brillouin zones. Phys Rev B 2015;91:94306. http://dx.doi.org/10.1103/PhysRevB.91.094306.
[22] Giannozzi P, Baroni S, Bonini N, Calandra M, Car R, Cavazzoni C, et al. QUANTUM ESPRESSO: a modular and open-source software project for quantum simulations of materials. J PhysCondens Matter 2009;21:395502.
[23] Garrity KF. First-principles search for n-type oxide, nitride, and sulfide thermoelectrics. Phys Rev B 2016;94:45122.
[24] Guo S-D. Biaxial strain tuned thermoelectric properties in monolayer PtSe 2. J Mater Chem C 2016;4:9366–74.
[25] Seko A, Togo A, Hayashi H, Tsuda K, Chaput L, Tanaka I. Prediction of low-thermal-conductivity compounds with first-principles anharmonic lattice-dynamics calculations and Bayesian optimization. Phys Rev Lett 2015;115:205901.
[26] Joshi H, Rai DP, Deligoz E, Ozisik HB, Thapa RK. The electronic and thermoelectric properties of a d2/d0 type tetragonal half-Heusler compound, HfSiSb: a FP-LAPW method. Mater Res Express 2017;4:105506.
[27] Whalley LD, Skelton JM, Frost JM, Walsh A. Phonon anharmonicity, lifetimes, and thermal transport in CH3 NH3 PbI3 from many-body perturbation theory. Phys Rev B 2016;94:220301.
[28] Reuss A. Calculation of the flow limits of mixed crystals on the basis of the plasticity of monocrystals. Z Angew Math Mech 1929;9:49–58.
[29] Voigt W. Lehrbuch der kristallphysik (mit ausschluss der kristalloptik). Springer-Verlag; 2014.

[30] Hill R. The elastic behaviour of a crystalline aggregate. Proc Phys Soc Sect A 1952;65:349.

[31] Fine ME, Brown LD, Marcus HL. Elastic constants versus melting temperature in metals. Scr Metall 1984;18:951–6.

[32] Pugh SF. XCII. Relations between the elastic moduli and the plastic properties of polycrystalline pure metals, London, Edinburgh, Dublin Philos. Mag J Sci 1954;45:823–43.

[33] Chung DH, Buessem WR, Vahldiek FW, Mersol SA. Anisotropy in single crystal refractory compounds. New York: Plenum; 1968. p. 328.

[34] Zener C. Elasticity and anelasticity of metals. University of Chicago press; 1948.

[35] Chen X-Q, Niu H, Li D, Li Y. Modeling hardness of polycrystalline materials and bulk metallic glasses. Intermetallics 2011;19:1275–81.

[36] Elliott RS, Triantafyllidis N, Shaw JA. Stability of crystalline solids—I: continuum and atomic lattice considerations. J Mech Phys Solids 2006;54:161–92.

[37] Togo A, Tanaka I. First principles phonon calculations in materials science. Scr Mater 2015;108:1–5.

[38] Anderson OL. A simplified method for calculating the Debye temperature from elastic constants. J Phys Chem Solids 1963;24:909–17.

[39] Kaur K. TiPdSn: a half Heusler compound with high thermoelectric performance. EPL Europhys Lett 2017;117:47002.

[40] Guo S-D. Importance of spin–orbit coupling in power factor calculations for half-Heusler ANiB (A= Ti, Hf, Sc, Y; B Sn, Sb, Bi). J Alloy Compd 2016;663:128–33.

[41] Zeeshan M, Singh HK, van den Brink J, Kandpal HC. Ab initio design of new cobalt-based half-Heusler materials for thermoelectric applications. Phys Rev Mater 2017;1:75407.

[42] Thomas JA, Turney JE, Iutzi RM, Amon CH, McGaughey AJH. Predicting phonon dispersion relations and lifetimes from the spectral energy density. Phys Rev B 2010;81:81411.

[43] Bardeen J, Shockley W. Deformation potentials and mobilities in non-polar crystals. Phys Rev 1950;80:72.

[44] Jacoboni C. Theory of electron transport in semiconductors: a pathway from elementary physics to nonequilibrium Green functions. Springer Science & Business Media; 2010.

[45] González-Romero RL, Antonelli A. Estimating carrier relaxation times in the Ba 8 Ga 16 Ge 30 clathrate in the extrinsic regime. PCCP 2017;19:3010–8.

[46] Samsonidze G, Kozinsky B. Half-Heusler compounds for Use in thermoelectric. Generators 2015.